Investigation of microvascular morphological measures for skeletal muscle tissue oxygenation by image-based modelling in 3D

B. Zeller-Plumhoff · K. R. Daly · G. F. Clough · P. Schneider · T. Roose

the date of receipt and acceptance should be inserted later

Abstract The supply of oxygen in sufficient quantity is vital for the correct functioning of all organs in the human body, namely for skeletal muscle during exercise. Traditionally, microvascular oxygen supply capability is assessed by analysis of morphological measures on transverse cross-sections of muscle, e.g., capillary density or capillary-to-fibre ratio.

In this work we are investigating the relationship between microvascular structure and muscle tissue oxygenation in mice. Phase contrast imaging was performed using synchrotron radiation computed tomography (SR CT) to visualize red blood cells (RBCs) within the microvasculature in mouse soleus muscle. Image-based mathematical modelling of the oxygen diffusion from the red blood cells into the muscle tissue was subsequently performed, as well as a morphometric analysis of the microvasculature. The mean tissue oxygenation was then compared to morphological measures of the microvasculature.

RBC volume fraction and spacing (mean distance of any point in tissue to closest RBC) emerged as the best predictors for muscle tissue oxygenation, followed by length density (summed RBC length over muscle volume). The 2D measures of capillary density and capillary-to-fibre ratio ranked last. We therefore conclude, that in order to assess states of health of muscle tissue it

B. Zeller-Plumhoff
Helmholtz-Zentrum für Material- und Küstenforschung, Geesthacht, Germany
Bioengineering Research Group, Faculty of Engineering and the Environment, University of Southampton, Southampton, UK
Tel.: +49 (0)40 8998 6904
E-mail: berit.zeller-plumhoff@hzg.de

G. F. Clough
Faculty of Medicine, University of Southampton, Southampton, UK

B. Zeller-Plumhoff, K. R. Daly, P. Schneider and T. Roose
Bioengineering Research Group, Faculty of Engineering and the Environment, University of Southampton, Southampton, UK

is advisable to rely on 3D morphological measures rather than the traditional 2D measures.

Keywords microvasculature muscle oxygenation · image-based modelling

1 Introduction

Over the last decades, the number of non-communicable diseases, including diabetes, heart disease, renal disease, hypertension and stroke, has increased dramatically, accounting for 60% of deaths worldwide [Hanson *et al.*, 2011]. The development of such cardio-metabolic diseases is associated with changes in both macrovascular and microvascular networks in most organ systems of the body, including liver, heart and skeletal muscle. Skeletal muscle, which makes up almost half of a (healthy) individual's body mass [Segovia *et al.*, 2014], is one of the key tissues investigated in the origin and outcomes of cardio-metabolic disease. It is among the main consumers of oxygen in the human body, in particular during exercise, and thus relies heavily on oxygen to be provided by the microvasculature. The microvasculature is defined as those blood vessels that have a diameter smaller than 150 μm and whose primary function is the delivery of nutrients and oxygen to the tissue [Clough & Norman, 2011]. If the vascular structure changes, for instance due to vessel rarefication, peripheral vascular resistance may increase and/or tissue oxygen delivery may be impaired [Clough & Norman, 2011]. To understand the structure-function relation between microvascular morphology and disease a large body of research has been conducted applying a wide range disease models in diverse vascular beds. The morphology of the microvasculature is identified by a number of morphological measures which are often reported in the research of cardio-metabolic disease.

These morphological measures, which are measured on two-dimensional (2D) transverse and longitudinal cross-sections of the muscle tissue or images of scanning electron microscopy of macerated vascular networks, are used to describe the oxygen exchange capability of the microvascular network. The most frequently used measures are capillary density (number of capillaries per cross-sectional area), capillary-to-fibre ratio (number of capillaries per number of muscle fibers in cross-section) and capillary tortuosity (Euclidian distance of vessel end/branching points over total vessel segment length)[Zeller-Plumhoff *et al.*, 2017]. Differences in these quantitative morphometric measures are investigated between healthy and diseased individuals (animal or human) and assumed to be related to the disease. Tortuosity is strongly disputed as a measure of oxygen delivery capability and thought to be linked mainly to the muscle's contractile state via the sarcomere length [Poole *et al.*, 1992, Mathieu-Costello, 1987, Mathieu-Costello *et al.*, 1989, Poole *et al.*, 1989]. Other morphological measures investigated are length of the capillary network [Dapp *et al.*, 2004, Georgi *et al.*, 2011], length density (microvascular network length over muscle volume) [Benedict *et al.*, 2011], volume fraction (microvascular network volume over muscle volume) [Kondo *et al.*,

2011] and fractal dimension [Gazit *et al.*, 1995, Lorthois & Cassot, 2010]. Fractal dimension is a measure of self-similarity of a network, i.e., the structure can be broken down into smaller parts that are the same as the entire structure [Peitgen *et al.*, 1992]. Fractal dimension is however disputed as a measure as the interpretation of results is difficult in a physiological sense. It has been shown that tumour networks can be differentiated from normal networks using the fractal dimension [Gazit *et al.*, 1995, Lorthois & Cassot, 2010]. Some researchers have shown how results differed when considering the vascularization in 2D vs. three dimensions (3D) [Cebasek *et al.*, 2006, Janacek *et al.*, 2009, Cebasek *et al.*, 2010, Erzen *et al.*, 2011] and that the three-dimensional consideration lead to an increase in the ratio of length of adjacent capillaries over length of the muscle fibre of 40%. This suggests that the interpretation of 3D data using 2D measures instead of 3D measures can be misleading when predicting the muscle tissue oxygenation, as has previously been suggested by other researchers as well [Egginton *et al.*, n.d., Egginton & Turek, 1990]. However, little research has been performed to quantify the predictive power of either 2D or 3D morphological measures in terms of muscle tissue oxygenation. In addition to morphological measures, some investigators have suggested that the haematocrit, i.e., the ratio of red blood cell (RBC) over overall blood volume, was linked to the metabolic syndrome [Fraser *et al.*, 2013, 2015]. Additionally, McClatchey *et al.* [2017] have recently investigated the importance of perfused capillary density and perfusion heterogeneity. Their findings suggest that capillary density is only weakly related to skeletal muscle oxygenation, whereas capillary perfusion heterogeneity plays a larger role [McClatchey *et al.*, 2017]. In conclusion, it may be preferable to study measures quantifying the red blood cell distribution within the capillary network rather than morphological measures of the blood vessels themselves.

One key obstacle in linking 3D microvascular morphology and tissue oxygenation is the lack of imaging methods that can simultaneously provide *in vivo* information on oxygen concentration and penetrate the tissue sufficiently to obtain a map of the capillary network. An alternative approach is mathematical modelling, which can be used to simulate tissue oxygenation, based on images of the vascular network obtained *ex vivo*.

In this work we investigate the link between microvascular morphology and tissue oxygenation through image-based modelling informed by phase contrast imaging based on synchrotron radiation computed tomography (SR CT). We have visualized the red blood cells within the capillaries, from which we have computed the oxygen diffusion into the muscle tissue. We detail the methodology applied for animal preparation, imaging, image processing and finally for retrieving the morphological measures for the microvasculature, which is required for mathematical modelling of the oxygen diffusion process in the muscle tissue. This allowed us to relate the tissue oxygenation inferred from image-based mathematical modelling to the morphological measures of the microvasculature. We are thus presenting the first mathematical simulation of skeletal muscle tissue oxygenation based on images of red blood cells

within the muscle, as well as the first evaluation of morphological measures used in oxygenation prediction by means of mathematical modelling.

2 Methods

All animal procedures were in accordance with the regulations of the United Kingdom Animals (Scientific Procedures) Act 1986 and were conducted under Home Office Licence number 70-6457. The study received institutional approval from the University of Southampton Biomedical Research Facility Research Ethics Committee.
Male C57B/L6 mice (n=5) were maintained under controlled conditions. At 15 weeks of age the mice were killed by cervical dislocation. The soleus muscle of the right leg was dissected and fixed in 10% formaldehyde at 4°C overnight. It was then dehydrated in a graded series of methylated spirit and embedded in paraffin wax in coffin moulds. The wax block was trimmed for imaging using an industrial razor blade and glued onto a scanning electron microscopy stub that was clamped into a standard pin chuck (fig. 1).

2.1 Imaging

Scanning of the muscles using SR CT was performed at the TOMCAT beamline of the Swiss Light Source (SLS) at the Paul Scherrer Institut in Villigen, Switzerland. All scans were performed at 14 keV, at a voxel size of 0.77 μm, an exposure time of 180 ms, where 1601 projections were acquired over an angular range of 0°-180°. For each scan we additionally recorded 32 dark field and 160 flat field images to correct the raw projections. A non-zero propagation or sample-to-detector distance of 60 mm was chosen so that the free-space propagation of the (coherent) X-rays transforms the phase modulation into intensity variations providing image contrast, recorded as projections on the charge-coupled device (CCD) detector. The phase of the projection images was then retrieved using an in-house implementation of the Paganin single-distance non-iterative phase retrieval algorithm [Paganin *et al.*, 2002] and subsequently reconstructed using an in-house implementation [Marone & Stampanoni, 2012] of the Gridrec algorithm [Dowd *et al.*, 1999] at TOMCAT.

The muscles were considerably longer (~ 8 mm) than wide (~ 2 mm) and thus they exceeded the field of view (2x2 mm^2) of the detector at TOMCAT at the chosen spatial resolution along the rotation axis. Therefore, it was necessary to take a number of scans along the length of the muscle in order to be able to image the whole muscle. Depending on the straightness of the muscle and its total length, this resulted in 5-7 scans per muscle (including overlapping regions). After reconstruction a calibration was performed by linear transformation of the data histogram to match average greyscales of paraffin wax and muscle fibres in all subdatasets. See figure 1 for a sketch of the overlapping regions (blue dashed lines).

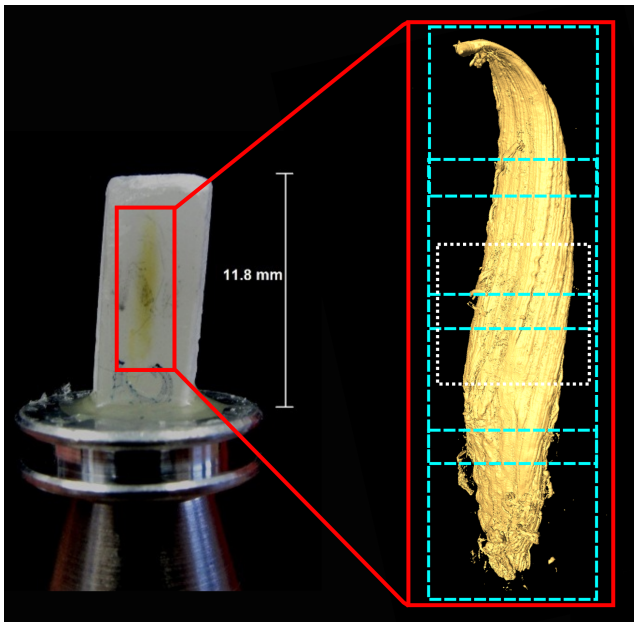

Fig. 1 Mounting of the sample and batch scanning. The muscles were considerably longer (~ 8 mm) than wide (~ 2 mm) and thus they exceeded field of view (2x2 mm^2) of the detector at TOMCAT, therefore, it was necessary to take a number of scans along the length of the muscle in order to be able to image the whole muscle (blue dashed regions). Due to the high computational effort, the regions for segmentation and modelling were limited to a cubic area from the muscle belly (white dotted region). Not to scale.

Imaging of RBCs through phase contrast was validated by direct comparison of the 3D SR CT images with 2D histological slides of the same muscle, which were stained with CD31 (ab28364, Abcam, dilution 1:150) for vascular endothelium to facilitate the detection of the RBCs present in capillaries, see figure 2. SR CT and histology images were correlated manually using the 'simple registration' tool in VGStudio Max 2.0 (Volume Graphics GmbH, Germany). To account for the thickness of the histological sections (4 μm), a maximum intensity projection over 7 SR CT slices was performed in Fiji [Schindelin *et al.*, 2012]. Counting of RBCs was then performed on both image types and the numbers were compared.

2.2 Image segmentation

Due to the computational load of processing the segmented dataset for modelling, the segmentation of each muscle was limited to a $(1.5mm)^3$ cube from the medial muscle region (white dotted region in fig. 1). As the oxygen supply to the tissue originates mainly from the capillaries only the red blood cells in the capillaries were segmented and not those in larger blood vessels.
To enhance the contrast between RBCs and muscle fibres a "bandpass fil-

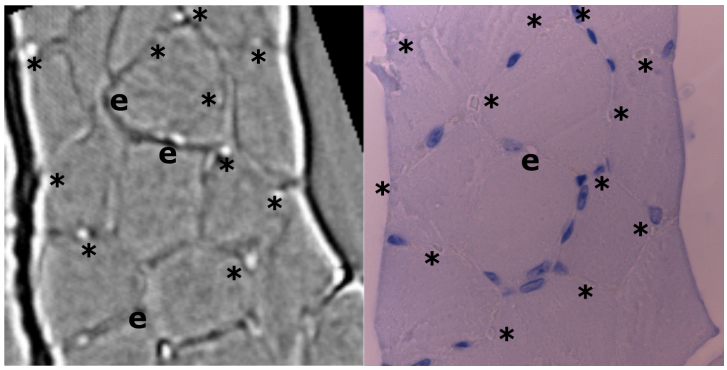

Fig. 2 Correlated SR CT and histology images (stained with CD31) for RBC validation. SR CT and histology images were visually correlated. To account for the thickness of the histological sections (4 μm), a maximum intensity projection over 7 SR CT slices was performed. SR CT images were bandpass filtered to highlight red blood cells (and muscle fibre edges). (*) highlights the RBCs counted for the comparison and (e) marks the empty capillaries.

ter" was applied in ImageJ [Schindelin *et al.*, 2012] with an upper and lower threshold of 3 px and 1 px, respectively. This resulted in highlighting all spatially fast-changing features, such as the RBCs and muscle fibre edges, as well as ring artefacts (originating e.g. from dead detector pixels). To reduce the image size and smooth the artefacts a 2x2x2 binning filter in ImageJ was subsequently applied. The resulting image was then binarised through absolute thresholding to segment bright features, i.e., the RBCs and muscle fibre edges (see fig. 2). This was performed in Avizo Fire 9.0 (FEI, USA). The chosen threshold was determined using a short parametric study of the influence of the threshold on the resulting number of detected red blood cells, such that the number of detected red blood cells per muscle cross-section was in the range described in the literature. Highlighted muscle fibre edges were manually selected using the "magic wand tool" in Avizo to subtract them from the segmentation. The region growing over all slices allowed for fast selection of the edges.

The muscle tissue was segmented semi-manually by tracing the edges of the muscle volume in Avizo in a number of slices and then connecting the segmented areas by linear interpolation between the slices. For simplicity, other soft tissues in skeletal muscle, such as nerves, were not segmented separately but added to the bulk muscle tissue.

2.3 Quantitative morphometry

For the quantification of morphological measures of the microvasculature (based on the segmented red blood cells), the binary image stacks obtained after segmentation of the RBCs and muscle tissue, respectively, were used. For the implementation of the procedures exlained below, an ImageJ plugin

was used for the skeletonization [Schindelin *et al.*, 2012] and the "Volume Fraction" BoneJ plugin [Doube *et al.*, 2010] for voxel counting.

Volumes and volume fraction Volume fraction was defined as the volume of the RBCs over the muscle volume. Muscle volume and RBC volume were computed by counting white voxels in the respective binary image. To determine the actual volume in mm^3 the counts were corrected for the voxel resolution. Division of both volumes provides the volume fraction of the microvasculature.

Surface area density The surface area density was defined as the ratio of RBC surface area over muscle volume. The surface area of the red blood cells could be computed as the sum of all RBC edge voxels. These were given after application of a Sobel edge detection filter on the RBC binary data. Counting of the voxels, multiplication by voxel size and division by muscle volume gave the surface area density.

Length density Length density was the length of the segmented RBC network over the muscle volume. To determine the length density of the RBC network (defined as overall length of RBCs over muscle volume) it was first necessary to skeletonize the RBC binary images, to reduce each RBC to its center line. Counting the remaining voxels in the image stack then equates to measuring the length of the RBC network. The multiplication by voxel size was performed and division by muscle volume as determined above.

Capillary density The number of capillaries (in this case RBCs) per muscle cross-sectional area is defined as the capillary density. The (binary) skeletonized RBC dataset was used to determine the number of red blood cells per slice by counting the number of voxels per slice. The count was divided by the muscle tissue area from the corresponding slice, which was obtained by counting voxels in the binary muscle volume dataset (and multiplication by voxel size). The counting was performed for three slices in the medial region of the muscle and the final number was obtained by averaging over these slices.

Capillary-to-fibre ratio The capillary-to-fibre ratio was defined as the number of RBCs over the number of muscle fibres per muscle cross-section. For the capillary-to-fibre ratio, the capillary numbers were obtained as for the capillary density. The number of muscle fibres in each slice was then determined by selecting the appropriate images from the original (non-binary) dataset and manually counting the number of muscle fibres. Division of the number of red blood cells by the number of muscle fibres gave the capillary-to-fibre ratio, which was averaged over three slices.

Fractal dimension In order to determine the fractal dimension no image processing steps needed to be applied. The binary RBC dataset was used to apply a (3D) box-counting algorithm. This was implemented by applying the BoneJ plugin "Fractal Dimension" [Doube *et al.*, 2010], which returns fractal dimension as well as the error of the fit.

RBC spacing RBC distribution within the muscle tissue was characterised using a spacing function. The mean distance to the next red blood cell (in 3D) for each point in the muscle tissue was computed. To this end, a distance map was created for the binary RBC image stack computing the distance from every voxel in the stack to the nearest RBC. Multiplication with the binary muscle volume image stack limited the distance map to the muscle tissue. The arithmetic mean of greyscales in the resulting dataset was taken as the mean RBC spacing. The distance map was created using the "3D distance map" plugin in ImageJ [Schindelin *et al.*, 2012].

2.3.1 Histological validation of capillary density and capillary-to-fibre ratio

For validation of the two morphological measures used in assessing microvascular oxygenation capability, i.e., capillary density and capillary-to-fibre ratio, we have performed lectin staining using fluorescein labelled Griffonia Simplicifolia lectin-1 (FL 1101, Vector Labs) on 7 C57B/L6 mouse soleus muscles. CD and C:F were computed in three areas of 1 mm^2 of one thin section from the muscle belly for each muscle.

2.4 Mathematical modelling of tissue oxygenation

For image-based modelling, ScanIP 4.4 (Simpleware Ltd, UK) was used to generate a surface mesh of RBCs and muscle tissue respectively. OpenFOAM, a free, open source CFD based on the programming language C [ope, 2016], was used as numerical solver. The surface mesh was extended into a finite element mesh by the OpenFOAM utility *snappyHexMesh*. ScanIP does also have the capability of producing FE meshes, but the computational load is significantly higher and it was not possible to produce an FE mesh of the segmented cube. In order to correctly mesh the small RBCs, it was necessary to refine the mesh around these by halving the size of all edges at least 5 times using *snappyHexMesh*, thus reducing the edge length from the order of 0.1 mm to nm. No refinement of the muscle surface was performed. The visualisation of the simulation results was performed in Paraview 5.1.2 (Kitware Inc., US and Los Alamos National Laboratory, US). The OpenFOAM model used in this work was based on the LaplacianFoam solver that was designed to solve a diffusion equation with constant diffusion coefficient and which we extended to include a non-linear consumption term. Full simulation details are available on request.

The diffusion of oxygen from the RBCs into the tissue where it is consumed was modelled using the diffusion-reaction equation

$$\frac{\partial C}{\partial t} = D\nabla^2 C - M(C) \qquad \text{in}\,\Omega_t\,, \tag{1}$$

where C is the molecular concentration in mol/m^3 at time t and D is the diffusion coefficient in m^2/s. The oxygen consumption was described by Michaelis-Menten kinetics $M(C) = \frac{M_0 C}{C+C_{50}}$ with $C_{50} = 8.1 \cdot 10^{-4}$mol/m^3 the muscle oxygen concentration at half demand and $M_0 = 15.7 \cdot 10^{-5}$mlO_2/(ml s) (shown in table 1).

Boundary conditions where applied at the RBC-tissue interface and the outer tissue boundary. The flux of oxygen from the RBCs into the tissue is described by a flow along its concentration gradient [Al-Shammari *et al.*, 2012, Goldman & Popel, 2001, 2000], and depends on the capillary permeability, which is characterized by the mass transfer coefficient k [Goldman, 2008]. Thus,

$$-\mathbf{n_v} \cdot (D\nabla C) = k(C_0 - C)\,, \tag{2}$$

where $\mathbf{n_v}$ is the unit normal vector to the vessel surface (pointing into the vessel), C_0 is the molecular concentration in mol/m^3 at time $t = 0$.

The boundary condition usually imposed at the outer tissue surface is a no-flux boundary condition, i.e.,:

$$\mathbf{n_o} \cdot D\nabla C = 0\,, \tag{3}$$

where $\mathbf{n_o}$ is the outer unit normal vector to the outer tissue surface. This implies that all oxygen supplied by the blood vessels in one muscle stays within this muscle.

Finally, as an initial condition we set

$$C = C_{cap} \quad \text{at} \quad t = 0\,, \tag{4}$$

with $C_{cap} = 3.24 \cdot 10^{-2}$ mol/m^3 the intra-capillary oxygen concentration (derived from table 1).

For implementation, the model dimensions were changed into $[C]$ = nmol/mm^3, such that in equation $k = 1$ mm/s. Furthermore, as $D/k << 1$ m the boundary condition in equation (2) was approximated as $C = C_0$. It was assumed that all RBCs were fully saturated with oxygen and remained so over time.

For the non-linear Michaelis-Menten it was necessary to use a mixed Crank-Nicolson and implicit Euler scheme to be able to solve the equation numerically. The solver was defined to be CrankNicolson 0.9 in the OpenFOAM library *fvSchemes*. The parameter $\phi = 0.9$ in this case defines the blending between both methods, with $\phi = 1$ being a pure Crank-Nicolson scheme and $\phi = 0$ a pure implicit Euler scheme ope [2016]. All other solver schemes were set to linear Gaussian interpolations.

The parameters used for modelling the diffusion and uptake of oxygen in muscle tissue have been summarised by Al-Shammari *et al.* [2012, 2014] and

Parameters defining the oxygen perfusion in muscle	Value	Source
O_2 Diffusion coefficient (37°C) [10^{-9}m^2/s] D	2.11	Levick [2003]
Consumption rate in muscle at rest [10^{-5} ml O_2/(ml s)] M_0	15.7	Wust *et al.* [2009]
Intracapillary PO_2 [mmHg] P_{cap}	20	Eggleton *et al.* [2000]
O_2 solubility [10^{-5} ml O_2/ (ml mmHg)] α	3.89	Goldman & Popel [1999]
O_2 capillary wall permeability [m/s] k	~ 10-3	Levick [2003]
Muscle PO_2 at half demand [mmHg] P_{50}	0.5	Honig & Gayeski [1982]

Table 1 Model parameters for modelling the diffusion and uptake of oxygen in skeletal muscle tissue as described by Al-Shammari *et al.* [2012, 2014]. The parameters are given in terms of tissue PO_2 and are converted into oxygen concentration C for model implementation.

can be found in table 1. Before integration into the model, all values were converted into a description as oxygen concentration C rather than oxygen partial presure P, by use of the oxygen solubility α.

For each muscle the mean oxygen concentration within the modelled cubic muscle volume was computed. In addition, the fraction of mesh cells with an oxygen concentration lower than C_{50} was determined to take into account the variation of the oxygenation across the whole muscle volume. Respective linear regression lines for the correlations were computed in Origin8.1 (which uses the least squares method), returning also the adjusted R^2 that determines the quality of the fit. R^2 was used to conclude which morphological measure best predicted the tissue oxygenation.

3 Results

3.1 Comparison between histology and SR CT

Figure 3 displays the result of the comparison of red blood cell identification between SR CT and histology images. The counting for CD31 by observer 1 is fitted by the line $0.91x + 0.58$ with $R^2 = 0.85, p < 0.001$. It was found that the number of misidentified red blood cells, i.e., those RBCs that were visible in one image but not the other, was lower than 10% and the overall number of RBCs identical when derived via histology or SR CT. Thus, using phase contrast-based SR CT it was possible to image red blood cells in mouse skeletal muscle on the whole organ scale. In order to assess the impact of error in RBC counting on the oxygenation computation, we have investigated a test cube of muscle from which we removed two percent and ten percent of RBCs, respec-

tively. The change in computed muscle oxygen concentration was found to be insignificant with 0.01% and 0.09%, respectively (see appendix for details).

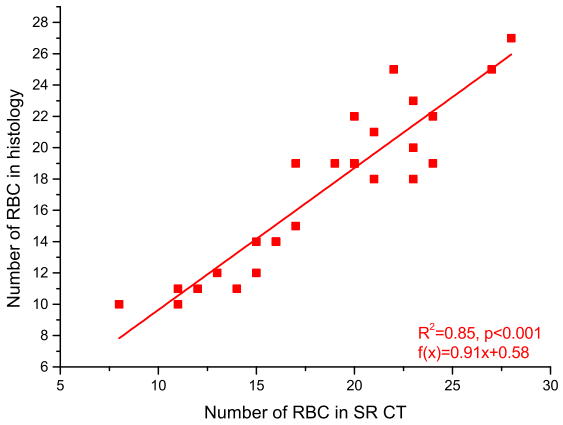

Fig. 3 Counts of red blood cells by an observer on SR CT slices vs. histology.

3.2 Quantitative morphometry of RBC networks

The mean quantitative morphometry of the RBC network based on the SR CT images was determined for all muscles, as well as the mean tissue oxygenation. Due to the naturally variable perfusion of capillaries with red blood cells the standard deviation of the different morphological measures is large. The mean red blood cell density was determined to be $828 \pm 155\,\mathrm{mm}^2$. The red blood cell-to-fibre ratio 0.90 ± 0.24. The average fractal dimension was found to be 2.53 ± 0.04 , the mean surface area density was $3.1 \pm 0.5\,\mathrm{mm}^{-1}$ and the mean length density was $875 \pm 130\,\mathrm{mm}^{-2}$. Finally, the mean volume fraction was determined as $6.5 \pm 1.1 \cdot 10^{-3}$ and the mean RBC spacing as $17.5 \pm 1.4\,\mu\mathrm{m}$.

3.2.1 Histological validation of capillary density and capillary-to-fibre ratio

The mean capillary density was computed to be 1211 ± 167 in the lectin stained thin sections of soleus muscle. The capillary-to-fibre ratio was determined as 0.1 ± 0.07.

3.3 Tissue oxygenation model

Figure 4 displays the results of the tissue oxygenation in the case of Michaelis-Menten kinetics for an exemplary muscle. The oxygen diffuses from the RBCs

(red) into the muscle where it is consumed.

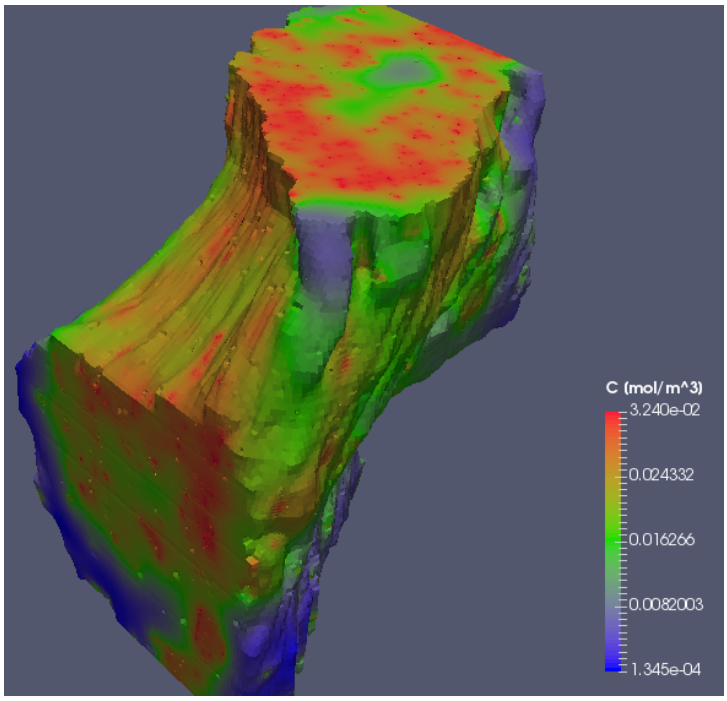

Fig. 4 Tissue oxygenation with Michaelis-Menten consumption in a cubic muscle volume. The oxygen diffuses from the red blood cells, where oxygen is at its highest concentration C, to the tissue where it is consumed.

To visualize the 3D nature of the data and computed oxygenation, a contour plot of the oxygenation of a smaller tissue cube is depicted in figure 5. The decrease in tissue oxygen concentration from the red blood cells outwards is visible. Regions with fewer RBCs present reach an overall lower value of concentration than those that are well perfused.

3.4 Relationship between tissue oxygenation and RBC network morphometry

The mean oxygen concentration and volume ratio of cells below C_{50} *vs.* each morphological measure and the respective fitted linear regression lines are displayed in figure 6.

The highest coefficient of determination was obtained for the relationship between volume fraction and mean oxygen concentration with $R^2 = 0.97$ followed by that for the mean distance to the next RBC (RBC spacing) with

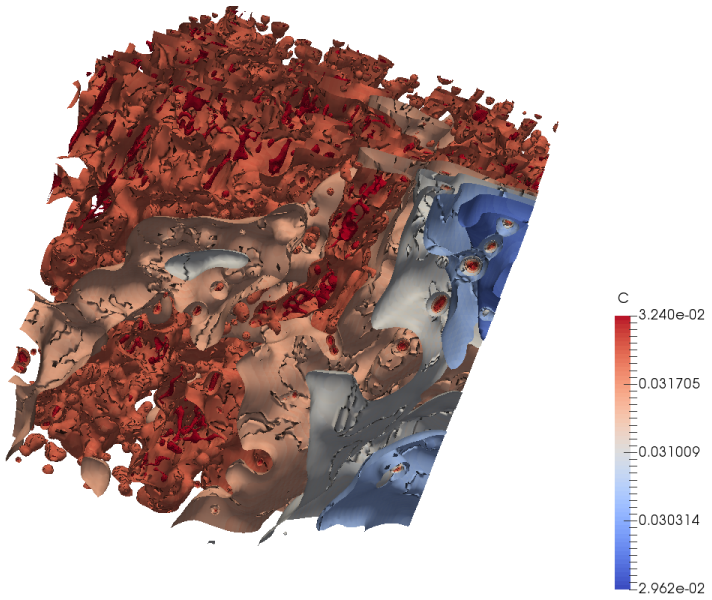

Fig. 5 Contour plot of tissue oxygenation with Michaelis-Menten consumption in a reduced cubic muscle volume. The oxygen diffuses from the red blood cells, where it is at its highest concentration, to the tissue where it is consumed.

$R^2 = 0.84$. The lowest coefficients of determination in terms of mean oxygen concentration were computed for capillary density ($R^2 = 0.17$) and capillary-to-fibre ratio ($R^2 = 0.26$). However, in the case of volume fraction of mesh cells with a concentration lower than C_{50} the relationships change. The correlation with RBC spacing remains strong ($R^2 = 0.88$), whilst that for volume fraction decreased to $R^2 = 0.59$. Length density and surface fraction remained nearly constant and were on a similar scale as volume fraction, with $R^2 = 0.52$ and $R^2 = 0.44$, respectively. The correlation for capillary density remained almost constant as well, whilst that for fractal dimension and capillary-to-fibre ratio diminished completely ($R^2 = 0.06$).

4 Discussion

In this study we have shown that the most successful morphological measures for the prediction of muscle tissue oxygenation are RBC volume fraction and RBC spacing. This stands in contrast to what is currently employed in research. Furthermore, this is the first study, where imaging of red blood cells within muscle tissue was possible using non-destructive, three-dimensional imaging, without application of contrast agents.

The average red blood cell density of $828 \pm 155\,\mathrm{mm}^2$ is in agreement with capillary density values found in the literature, especially for young mice

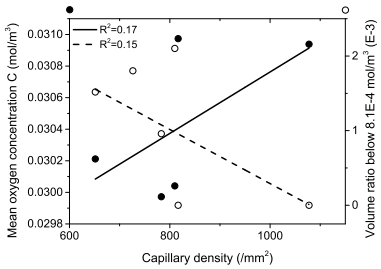

(a) Capillary density vs. mean oxygen concentration $R^2 = 0.17$ and vs. volume ratio with $C < C_{50}$ $R^2 = 0.15$

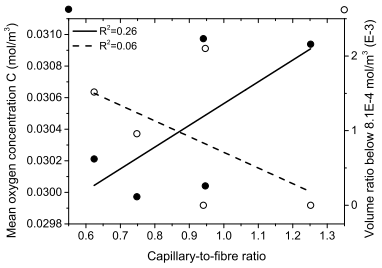

(b) Capillary-to-fibre ratio vs. mean oxygen concentration $R^2 = 0.26$ and vs. volume ratio with $C < C_{50}$ $R^2 = 0.06$

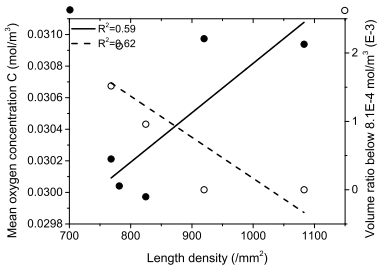

(c) Length density vs. mean oxygen concentration $R^2 = 0.59$ and vs. volume ratio with $C < C_{50}$ $R^2 = 0.52$

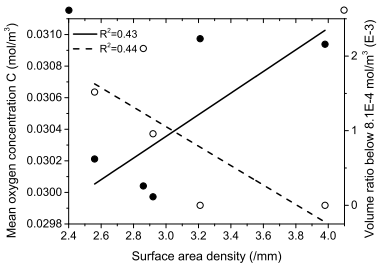

(d) Surface area density vs. mean oxygen concentration $R^2 = 0.43$ and vs. volume ratio with $C < C_{50}$ $R^2 = 0.44$

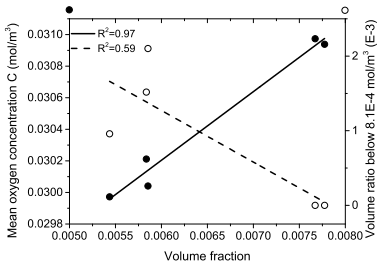

(e) Volume fraction vs. mean oxygen concentration $R^2 = 0.97$ and vs. volume ratio with $C < C_{50}$ $R^2 = 0.59$

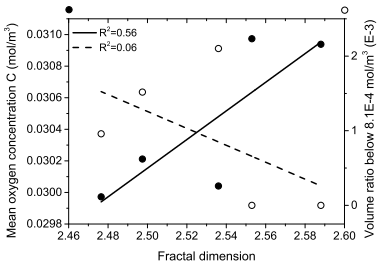

(f) Fractal dimension vs. mean oxygen centration $R^2 = 0.56$ and vs. volume ratio with $C < C_{50}$ $R^2 = 0.06$

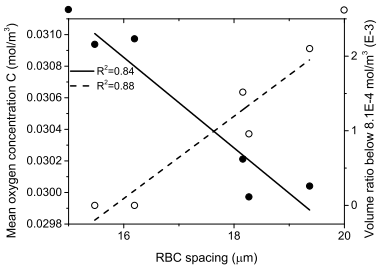

(g) RBC spacing vs. mean oxygen concentration $R^2 = 0.84$ and vs. volume ratio with $C < C_{50}$ $R^2 = 0.88$

Fig. 6 Relations between morphometric measures characterising the red blood cells and tissue oxygen concentration. The mean tissue oxygenation based on Michaelis-Menten kinetics has been plotted against the morphological measures. Additionally, the volume fraction of the cells with a concentration lower than C_{50} is shown. A linear regression line was fitted for each plot, including R^2. The strongest correlations are observed for measures of volume fraction and RBC spacing whilst capillary density, fractal dimension and capillary-to-fibre ratios were correlated to a lesser extent to tissue oxygenation.

($867 \pm 100\,\mathrm{mm}^2$ [Davidson *et al.*, 1999]). It is 28% lower than the capillary density computed from histological sections (1211 ± 167). This difference may however be due to the fact that not all capillaries are perfused with red blood cells at all times. The red blood cell-to-fibre ratio was determined as 0.90 ± 0.24 which is significantly lower than values found in the literature (> 1.8 Poole *et al.* [1989], Hudlicka [1985], Dapp *et al.* [2004]). However, histological validation that was performed showed a similar capillary-to-fibre ratio of 0.1 ± 0.07. This suggests that the value obtained by SR CT is representative of the capillary-to-fibre ratio in the particular breed of mouse. Furthermore, it is likely that the computed values for RBC density and RBC:F are lower than those found in the literature, as they are averaged over a larger volume of the muscle, whereas the values found in the literature are often taken from very small regions in the muscle belly. Capillary density and capillary-to-fibre ratios computed from belly regions of muscle have been found to differ from capillary density and capillary-to-fibre ratios computed from peripheral muscle regions [Murfee *et al.*, 2005].The average fractal dimension was 2.53 ± 0.04 which is slightly higher than fractal dimension reported in the literature Gazit *et al.* [1995], Masters [2004], Gould *et al.* [2011]. A difficulty in comparisons with the literature is that most authors do not describe the overall volume used to determine the fractal dimension, which influences the results in fractal box counting (the bigger the volume compared to the structure studied, the smaller the fractal dimension). Furthermore, the value of 2.53 ± 0.04 is in agreement with the values obtained by Peitgen *et al.* [1992] for 3D diffusion-limited growth processes ($2.4 - 2.5$), which suggests that the determined values are meaningful. The mean length density of $875 \pm 130\,\mathrm{mm}^{-2}$ was significantly lower than values found in the literature [Erzen *et al.*, 2011]. The reason for this is that by visualisation of RBCs in the blood vessels and not the blood vessels themselves and if the RBCs are not everywhere within the vessels, the length of the blood vessel network is underestimated. Moreover, the comparison with the literature is difficult if the standard stereological definition of length density was used rather than an adapted definition. Finally, the mean volume fraction of $6.5 \pm 1.1 \cdot 10^{-3}$ is lower than that obtained for the rat soleus muscle by one order of magnitude [Kondo *et al.*, 2011]. This, however, may be due to the difference between animals. No findings regarding volume fraction in mouse soleus muscle were published in the literature. Furthermore, no data was available on microvascular spacing or surface area densities. The quality of the morphological analysis of the structure of the microvasculature by visualisation of red blood cells depends on there being RBCs present in the capillaries. The number of capillaries that contain RBCs will vary with perfusion and haematocrit.

From the computed fits for the morphological measure vs. oxygenation relationships it follows that 3D measures were more closely related to muscle tissue oxygenation (except fractal dimension) than the 2D measures capillary density and capillary-to-fibre ratio. This has been expected, as the 2D measures fail to incorporate 3D volumetric information of the microvascular structure as provided by the 3D CT data. This effect becomes more pronounced when

we regard the correlation of the morphological measure with the volume fraction of those mesh cells that are below C_{50}, which is the muscle oxygen concentration at half demand at rest. During exercise this correlation is expected to become even stronger, as the oxygen demand increases significantly. The capillary-to-fibre ratio does not take into account any area or volume of tissue oxygenation, thus performing poorly in predicting tissue oxygenation, especially in terms of variation of oxygenation, as does the fractal dimension measure. The power of the capillary density to predict oxygen supply is likely to increase if it were to be computed over a larger number of CT slices, as variations in 3D (which are significant as shown by Murfee *et al.* [2005]) would then be taken into account. However, it would still only take into account the number of oxygen exchange locations (RBCs or capillaries) in each slice and not the actual exchange surface, which was shown in this study to be a better predictor for the overall oxygen exchange and thus tissue oxygenation. Finally, the mean distance to the next RBC (in 3D) expectedly emerged as one of the best predictors for tissue oxygenation, as the tissue oxygenation was governed by diffusion and thus mainly depending on the diffusion distance. A stronger correlation might result if the mathematical model took into account the soft tissues present in the muscle other than muscle fibres. To this end, the oxygen consumption of nervous tissue and interstitial tissues, as well as the oxygen diffusivity in these, need to be determined and the respective tissues would require segmentation for the modelling. Overall, the presented results are in good agreement with the theoretical modelling considerations recently presented by McClatchey *et al.* [2017]. In this study, the supply of oxygen to muscle tissue as modelled by the visualisation of red blood cells is realistic and withstands the application of oxygen uptake. Whilst it is unrealistic for all red blood cells present in the muscle to be fully saturated with oxygen to be supplied to the tissue, it is a first approximation of the reality.

From the comparison between SR CT images and histology it follows that SR CT is suited to identify the location of blood vessels with the number of misidentified red blood cells being lower than 10%. This number may however be overestimated as the correlation between histological slides and SR CT images is error prone, considering the small size of the RBCs. It is important to find the optimal set of rotations to correlate the images, as well the right SR CT slices over which the maximum intensity projection was applied, in order to minimize the difference between correlated SR CT and histology images. In validating features between SR CT slices and histology slices, the optimal alignment of these is the main challenge and much time was therefore spent in this process. Furthermore, it needs to be noted that a potential bias in counting by the observer cannot be excluded. However, the computation run on a test cube showed that an error of ten percent in number of RBCs resulted in an insignificant change of muscle oxygenation (see appendix). Therefore, we conclude that the results of this study are indeed predictive.

The method of overlaying these slices may not be ideal, possibly a method averaging the greyscales in each slice would achieve a more appropriate

comparison than the maximum intensity projection. This averaging could be weighted depending on their position in the 7-slice stack to account for the focus of the light microscope. Finally, the application of the bandpass filter to the phase retrieved SR CT images not only highlights the RBCs but also all edges of muscle fibres and empty capillaries, which can lead to misidentification of some RBCs. This however is a minor complication as the misidentification can be expected to be consistent over all slices, thus the overall slope the linear regression would change, yet the consistency of results remains.
Errors in the comparison may be induced during the processing of the samples for staining, e.g., microtoming the samples resulted in shearing artefacts. Such errors in processing are however intrinsic in the process of microtoming and histological staining and can not be entirely circumvented.

Solving the mathematical model numerically was computationally very expensive. It required 8 computing nodes with 12 processors each and between 15 to 72 hours for the non-linear consumption function to be solved using the mixed Crank-Nicolson scheme. The process of segmentation was time intensive, requiring at least 2-3 days per muscle cube.

Overall, we have presented the first mathematical simulation of skeletal muscle tissue oxygenation based on images of red blood cells within the muscle. It is also the first study on 3D image data that has not been artificially created investigating the link between morphological measures and muscle tissue oxygenation. We conclude that the measures of capillary density and capillary-to-fibre ratio, which are widely used in biological research to predict tissue oxygenation and thus states of tissue health, should be critically rethought and three-dimensional imaging and analysis methods ought to be used more frequently in pre-clinical research. If 2D measures of oxygenation are used they should be assessed in a series of defined transections along the whole length of the muscle. Furthermore, *ex vivo* techniques and assessment should be supported using 3D *in vivo* experimental data and/or results from computational modelling.

5 Appendix

A cubic testvolume of 200x200x200 pixels was extracted from a segmented muscle volume. The segmented red blood cells were labelled by connectivity using Avizo 9.2. This resulted in overall 7990 red blood cells in the muscle subvolume. A Matlab R2016a (The MathWorks Inc., USA) script was then used to remove two percent and ten percent of red blood cells randomly. The resulting datasets were meshed as explained above and the muscle oxygenation was computed. We found that the mean oxygen concentration in the muscle was changed by 0.01% after removing two percent of RBCs and by 0.09% after removal of ten percent of RBCs. The minimal concentration of oxygen changed by 0.08% and 0.07%, respectively.

Acknowledgements The authors would like to acknowledge funding by the Engineering and Physical Sciences Research Council (EPSRC) for the EPSRC doctoral training grant of author B. Zeller-Plumhoff and the British Heart Foundation for grant PG/12/18/29453. All SR CT imaging data was obtained at the Swiss Light Source (SLS). We acknowledge the Paul Scherrer Institut, Villigen, Switzerland for provision of synchrotron radiation beamtime at the TOMCAT beamline of the SLS and would like to thank Pablo Villanueva and Alessandra Patera for their assistance. Furthermore, we thank Jenny Norman, Jon Ward and Susan Wilson for enabling immunohistochemistry staining for the comparison between SR CT and histology data. The authors would also like to acknowledge Katherine Gould for her assistance in the preparation and staining of tissue for immunofluorescence counting for histological validation. We further acknowledge the use of the IRIDIS High Performance Computing Facility, and associated support services at the University of Southampton, in the completion of this work. Finally, we would like to thank Prof. Ian Sinclair for the valuable discussions that enabled our work and the μ-VIS X-ray Imaging Centre at the University of Southampton for providing the tools for image processing as well as data visualisation and evaluation.

References

OpenFOAM Website 2016. *http://www.openfoam.com/*.

Al-Shammari, A. A., Gaffney, E. A., & Egginton, S. 2012. Re-evaluating the Use of Voronoi Tessellations in the Assessment of Oxygen Supply from Capillaries in Muscle. *Bulletin of Mathematical Biology*, **74**(9), 2204–2231.

Al-Shammari, A. A., Gaffney, E. A., & Egginton, S. 2014. Modelling capillary oxygen supply capacity in mixed muscles: capillary domains revisited. *J Theor Biol*, **356**, 47–61.

Benedict, K. F., Coffin, G. S., Barrett, E. J., & Skalak, T. C. 2011. Hemodynamic Systems Analysis of Capillary Network Remodeling During the Progression of Type 2 Diabetes. *Microcirculation*, **18**(1), 63–73.

Cebasek, V., Radochova, B., Ribaric, S., Kubinova, L., & Erzen, I. 2006. Nerve injury affects the capillary supply in rat slow and fast muscles differently. *Cell Tissue Res*, **323**(2), 305–12.

Cebasek, V., Erzen, I., Vyhnal, A., Janacek, J., Ribaric, S., & Kubinova, L. 2010. The estimation error of skeletal muscle capillary supply is significantly reduced by 3D method. *Microvascular Research*, **79**(1), 40–46.

Clough, G. F., & Norman, M. 2011. The Microcirculation: A Target for Developmental Priming. *Microcirculation*, **18**(4), 286–297.

Dapp, C., Schmutz, S., Hoppeler, H., & Fluck, M. 2004. Transcriptional reprogramming and ultrastructure during atrophy and recovery of mouse soleus muscle. *Physiol Genomics*, **20**(1), 97–107.

Davidson, Y. S., Clague, J. E., Horan, M. A., & Pendleton, N. 1999. The effect of aging on skeletal muscle capillarization in a murine model. *J Gerontol A Biol Sci Med Sci*, **54**(10), B448–51.

Doube, M., Klosowski, M. M., Arganda-Carreras, I., Cordelieres, F. P., Dougherty, R. P., Jackson, J. S., Schmid, B., Hutchinson, J. R., & Shefelbine, S. J. 2010. BoneJ: Free and extensible bone image analysis in ImageJ. *Bone*, **47**(6), 1076–9.

Dowd, B. A., Campbell, G. H., Marr, R. B., Nagarkar, V., Tipnis, S., Axe, L., & Siddons, D. P. 1999. Developments in synchrotron x-ray computed

microtomography at the National Synchrotron Light Source. *Developments in X-Ray Tomography Ii*, **3772**, 224–236.

Egginton, S, & Turek, Z. 1990. Comparative Distributions of Numerical and Areal Indices of Tissue Capillarity | SpringerLink. *Oxygen Transport to Tissue XII*, 161–169.

Egginton, S., Turek, Z., & Hoofd, L. J. Differing patterns of capillary distribution in fish and mammalian skeletal muscle. *Respir Physiol*, **74**(3), 383–96.

Eggleton, C. D., Vadapalli, A., Roy, T. K., & Popel, A. S. 2000. Calculations of intracapillary oxygen tension distributions in muscle. *Mathematical Biosciences*, **167**(2), 123–143.

Erzen, I., Janacek, J., & Kubinova, L. 2011. Characterization of the capillary network in skeletal muscles from 3D data. *Physiol Res*, **60**(1), 1–13.

Fraser, G. M., Goldman, D., & Ellis, C. G. 2013. Comparison of Generated Parallel Capillary Arrays to Three-Dimensional Reconstructed Capillary Networks in Modeling Oxygen Transport in Discrete Microvascular Volumes. *Microcirculation*, **20**(8), 748–763.

Fraser, G. M., Morton, J. S., Schmidt, S. M., Bourque, S., Davidge, S. T., Davenport, M. H., & Steinback, C. D. 2015. Reduced uterine perfusion pressure decreases functional capillary density in skeletal muscle. *Am J Physiol Heart Circ Physiol*, **309**(12), H2002–7.

Gazit, Y., Berk, D. A., Leunig, M., Baxter, L. T., & Jain, R. K. 1995. Scale-invariant behavior and vascular network formation in normal and tumor tissue. *Phys Rev Lett*, **75**(12), 2428–2431.

Georgi, M. K., Vigilance, J., Dewar, A. M., & Frame, M. D. 2011. Terminal arteriolar network structure/function and plasma cytokine levels in db/db and ob/ob mouse skeletal muscle. *Microcirculation*, **18**(3), 238–51.

Goldman, D. 2008. Theoretical Models of Microvascular Oxygen Transport to Tissue. *Microcirculation*, **15**(8), 795–811.

Goldman, D., & Popel, A. S. 1999. Computational modeling of oxygen transport from complex capillary networks. Relation to the microcirculation physiome. *Adv Exp Med Biol*, **471**, 555–63.

Goldman, D., & Popel, A. S. 2000. A computational study of the effect of capillary network anastomoses and tortuosity on oxygen transport. *Journal of Theoretical Biology*, **206**(2), 181–194.

Goldman, D., & Popel, A. S. 2001. A computational study of the effect of vasomotion on oxygen transport from capillary networks. *Journal of Theoretical Biology*, **209**(2), 189–199.

Gould, D. J., Vadakkan, T. J., Poche, R. A., & Dickinson, M. E. 2011. Multifractal and Lacunarity Analysis of Microvascular Morphology and Remodeling. *Microcirculation*, **18**(2), 136–151.

Hanson, M., Godfrey, K. M., Lillycrop, K. A., Burdge, G. C., & Gluckman, P. D. 2011. Developmental plasticity and developmental origins of non-communicable disease: Theoretical considerations and epigenetic mechanisms. *Progress in Biophysics & Molecular Biology*, **106**(1), 272–280.

Honig, C. R., & Gayeski, T. E. 1982. Correlation of O2 transport on the micro and macro scale. *Int J Microcirc Clin Exp*, **1**(4), 367–80.

Hudlicka, O. 1985. Development and Adaptability of Microvasculature in Skeletal-Muscle. *Journal of Experimental Biology*, **115**(Mar), 215–228.

Janacek, J., Cebasek, V., Kubinova, L., Ribaric, S., & Erzen, I. 2009. 3D Visualization and Measurement of Capillaries Supplying Metabolically Different Fiber Types in the Rat Extensor Digitorum Longus Muscle During Denervation and Reinnervation. *Journal of Histochemistry & Cytochemistry*, **57**(5), 437–447.

Kondo, H., Fujino, H., Murakami, S., Nagatomo, F., Roy, R. R., & Ishihara, A. 2011. Regressed three-dimensional capillary network and inhibited angiogenic factors in the soleus muscle of non-obese rats with type 2 diabetes. *Nutr Metab (Lond)*, **8**(1), 77.

Levick, J. Rodney. 2003. *An introduction to cardiovascular physiology*. 4th edn. London: Arnold.

Lorthois, S., & Cassot, F. 2010. Fractal analysis of vascular networks: insights from morphogenesis. *J Theor Biol*, **262**(4), 614–33.

Marone, F., & Stampanoni, M. 2012. Regridding reconstruction algorithm for real-time tomographic imaging. *J Synchrotron Radiat*, **19**(Pt 6), 1029–37.

Masters, B. R. 2004. Fractal analysis of the vascular tree in the human retina. *Annu Rev Biomed Eng*, **6**, 427–52.

Mathieu-Costello, O. 1987. Capillary tortuosity and degree of contraction or extension of skeletal muscles. *Microvasc Res*, **33**(1), 98–117.

Mathieu-Costello, O., Hoppeler, H., & Weibel, E. R. 1989. Capillary tortuosity in skeletal muscles of mammals depends on muscle contraction. *J Appl Physiol (1985)*, **66**(3), 1436–42.

McClatchey, P Mason, Frisbee, Jefferson C., & Reusch, Jane E. B. 2017. A Conceptual Framework for Predicting and Addressing the Consequences of Disease-Related Microvascular Dysfunction. *Microcirculation*, n/a–n/a.

Murfee, Walter L., Hammett, Laura A., Evans, Caroline, Xie, Liqin, Squire, Maria, Rubin, Clinton, Judex, Stefan, & Skalak, Thomas C. 2005. High-frequency, low-magnitude vibrations suppress the number of blood vessels per muscle fiber in mouse soleus muscle. *Journal of Applied Physiology*, **98**(6), 2376–2380.

Paganin, D., Mayo, S. C., Gureyev, T. E., Miller, P. R., & Wilkins, S. W. 2002. Simultaneous phase and amplitude extraction from a single defocused image of a homogeneous object. *Journal of Microscopy-Oxford*, **206**, 33–40.

Peitgen, Heinz-Otto, JÃ¼rgens, Hartmut, & Saupe, Dietmar. 1992. *Chaos and fractals : new frontiers of science*. New York: Springer.

Poole, D. C., Mathieu-Costello, O., & West, J. B. 1989. Capillary tortuosity in rat soleus muscle is not affected by endurance training. *Am J Physiol*, **256**(4 Pt 2), H1110–6.

Poole, D. C., Batra, S., Mathieucostello, O., & Rakusan, K. 1992. Capillary Geometrical Changes with Fiber Shortening in Rat Myocardium. *Circulation Research*, **70**(4), 697–706.

Schindelin, J., Arganda-Carreras, I., Frise, E., Kaynig, V., Longair, M., Pietzsch, T., Preibisch, S., Rueden, C., Saalfeld, S., Schmid, B., Tinevez, J. Y., White, D. J., Hartenstein, V., Eliceiri, K., Tomancak, P., & Cardona, A. 2012. Fiji: an

open-source platform for biological-image analysis. *Nature Methods*, **9**(7), 676–682.

Segovia, S. A., Vickers, M. H., Gray, C., & Reynolds, C. M. 2014. Maternal obesity, inflammation, and developmental programming. *Biomed Res Int*, **2014**, 418975.

Wust, R. C., Gibbings, S. L., & Degens, H. 2009. Fiber capillary supply related to fiber size and oxidative capacity in human and rat skeletal muscle. *Adv Exp Med Biol*, **645**, 75–80.

Zeller-Plumhoff, B., Roose, T., Clough, G. F., & Schneider, P. 2017. Image-based modelling of skeletal muscle oxygenation. *Journal of The Royal Society Interface*, **14**(127).